Development of label-free biophysical markers in osteogenic maturation

Alice Bartolozzi[1,3], Federica Viti[1], Silvia De Stefano[1], Francesca Sbrana[1,2], Loredana Petecchia[1], Paola Gavazzo[1], Massimo Vassalli[1]

1. Institute of Biophysics, National Research Council of Italy, Genoa - Italy
2. Schaefer South-East Europe Srl, Rovigo – Italy
3. Dipartimento di Ingegneria dell'Informazione, Università di Firenze, Florence - Italy

Abstract

The spatial and temporal changes of morphological and mechanical properties of living cells reflect complex functionally-associated processes. Monitoring these modifications could provide a direct information on the cellular functional state. Here we present an integrated biophysical approach to the quantification of the morphological and mechanical phenotype of single cells along a maturation pathway. Specifically, quantitative phase microscopy and single cell biomechanical testing were applied to the characterization of the maturation of human foetal osteoblasts, demonstrating the ability to identify effective label-free biomarkers along this fundamental biological process.

Keywords

Human foetal osteoblasts; cell morphology characterization; cell mechanics investigation

Introduction

Label-free approaches in tissues, cells and molecular biology are nowadays particularly appealing, as testified by many recent publications (Ray and Steckl 2019, Golfier et al. 2017, Stern et al. 2009, Chang et al. 2017), due to their minimal invasiveness, maintenance of living cells (being therefore available for reuse and time series experimental designs), user-friendliness and rapidity. To such an extent, the analysis of mechanical and morphological features of single cells is gaining more and more relevance, having shown a tight correlation with the functional state of the cell in several conditions (Chen et al. 2016; Muthukumaran et al. 2012). For example, it is well known that cell mechanical behaviour is related to cancer staging (Kawano et al. 2015, Fortier et al. 2016), metastatic condition (Kumar and Weaver 2009, Brodland and Veldhuis 2012) and differentiation (Engler et al. 2006). Analogously, cell morphometric phenotyping has been fruitfully exploited, among the others, in cancers (Wu et al. 2015), blood pathologies (Ford 2013), and cellular transdifferentiation evaluation (Petecchia et al. 2016).

Over the past decade, many strategies and techniques have been proposed to support the characterization of biological samples down to the single cell level, either from the mechanical or morphological point of view. Among proposed approaches (Darling and Di Carlo 2015), Atomic

Force Microscopy (AFM) is certainly the most adopted and effective to identify mechanical signatures of cellular systems (Lulevich et al. 2006). In this paper, a similar approach is proposed, based on a recent implementation of the cantilever-based force measuring method used in AFM, but exploiting an innovative in-fiber detection method (Chavan et al. 2012). This device, nowadays converted in a commercial product (Piuma Chiaro, Optics11, The Netherland), provides much higher versatility and throughput measurements than standard AFM, still retaining the force resolution required to finely assess mechanical properties of single cells.

For what concerns the assessment of morphological features, most of the commonly exploited techniques foresee cells treatment and labelling (Monteiro et al. 2015), while white-light phase contrast microscopy requires complex and cumbersome image processing steps to provide a sensible quantitative description of the cell morphology (Ambühl et al. 2012). To overcome these intrinsic limitations of standard approaches, label-free quantitative phase imaging has emerged as a potential tool for efficient cell morphometry, also providing the possibility of cells reuse for successive evaluations (Zhang et al. 2018). In this paper, morphological aspects of living cells were evaluated qualitatively and quantitatively, respectively, through a non-interferometric approach based on the transport-of-intensity equation (TIE, Teague 1983) and using digital holography (Gabor, 1948).

Ossification is a complex and delicate physiological process, whose impairment might lead to the onset of potentially severe disorders, such as calcification of heart valve or osteoporosis (Rutkovskiy et al. 2016). Moreover, bone is a tissue intrinsically subjected to wide mechanical stimuli which represent the driving force of its continuous remodelling (Thompson et al. 2012) and single cells involved in this process are expected to experience a drastic change in the mechanical and morphological phenotype during maturation. Here this aspect was addressed focusing on a specific cell line, hFOB 1.19 (ATCC® CRL11372™ from ATCC, Manassas, VA, USA, from now on referred to as hFOB). hFOB is an immortalized cell line of human foetal osteoblasts from limb tissue of a spontaneous miscarriage, transfected with the temperature sensitive expression vector pUCSVtsA58 which alternatively enables cell proliferation or differentiation according to culture temperature (respectively 33.5°C and 39.5°C) (Harris et al. 1995). According to Yen et al. (2007) hFOB cells show multilineage differentiation potential and share several surface markers with stem cells from the stroma of the bone marrow. Due to their potential, hFOB cell line is commonly used as a model system for studying human osteoblast maturation, osteoblast physiology, and effects of biomolecular and chemical factors on osteoblast function and maturation. In the described work, hFOB was considered as the model for identifying novel label-free biomarkers to monitor the transition between immature and mature osteoblasts, therefore representing valuable indicators of the osteoblasts developmental stage.

Materials and methods

Cell culture

hFOB 1.19 cells are foetal osteoblasts taken from limb tissue and therefore already in a specific developmental pathway. Nevertheless hFOB cells show a multilineage differentiation potential and share several surface markers with stem cells from the stroma of the bone marrow (Yen et al. 2007). Being immortalized with a temperature-sensitive SV40 large T antigen, this cell line is able to proceed towards cell proliferation when cultured at 33.5°C in a humidified atmosphere of 5% CO2, or cell differentiation towards mature osteoblasts when grown at 39.5°C, without the need to add any chemical supplement in the cell culture medium. hFOB cell line was cultured in accordance with ATCC recommendations. The base medium was a 1:1 mixture of Ham's F12 Medium Dulbecco's Modified Eagle's Medium, (DMEM-Ham's F-12, GIBCO), with 2.5mM L-glutamine (Sigma-Aldrich, St Louis, MO, USA), without phenol red. To complete the growth medium, G418 (0.3 mg/mL) and 10% foetal bovine serum (FBS) (Sigma-Aldrich) were added to the base medium. Medium was changed every three days. For all experiments, the same passage, from 2 to 10, was used.

Experimental design

hFOB were monitored in the following conditions, each considered in at least three replicates: during the proliferation, with cells growing at 33.5°C, (case A); during maturation toward the osteoblastic phenotype, moving cells at 39.5°C for 15 days, and performing functional and morpho-mechanical tests at day 5 (case B), day 11 (case C), and day 15 (case D). The actual maturation of the cell line was assessed through several traditional indicators of the osteoblastic phenotype, and on top of this, morpho-mechanical experiments were carried out. In detail, for each experimental condition, the following readouts were evaluated: functional information related to osteogenic maturation towards bone phenotype including (1) *calcium deposition,* assessed by Alizarin Red S (Alizarin), (2) *osteocalcin expression,* evaluated through confocal microscopy (CM), and (3) *gene targets expression,* defined by means of qPCR; *quantitative* and *qualitative cell morphology,* assessed respectively by (4) digital holographic microscopy (DH) and (5) quantitative phase imaging based on transport of intensity equation resolution (TIE), to shed light on the morphological changes consequent to experimental conditions; and (6) *mechanical properties*, by single cell Chiaro nanoindenter, to reveal elastic response in difference culture condition. Functional assessments, together with TIE results, were performed to check osteoblasts maturation trend, while DH images and nanoindentations returned phenotypical modifications related to cellular evolution.

Osteogenic staining

Calcium deposition was assessed by staining with Alizarin Red S (Petecchia et al. 2015). Briefly, hFOB grown on glass cover slips were fixed in 4% paraformaldehyde (PFA), and stained with 2% aqueous solution of Alizarin red S (Sigma Aldrich) for 10 minutes at room temperature.

In order to evaluate osteocalcin expression, cells were grown on cell culture dish (format: Ø 35 mm) with glass bottom for microscopic applications (Greiner Bio-One International, supplier: Savatec SRL, Torino, Italy), fixed in 4% PFA at room temperature, permeabilised with 0.2% Triton X-100 and blocked with 20% normal goat serum (Vector, Labs Burlingame, CA, USA) for 1 h at room temperature. Then cells were incubated with mouse anti-human osteocalcin (1:50 Santa Cruz Biotechnology), washed and incubated with Alexa-fluor 633 (red) goat anti-rabbit (Molecular Probes) (Petecchia et al. 2015). Image cells were acquired by confocal laser scanning microscopy (TCS SL microscope; Leica; Mannheim, Germany), using a 20X PL APO N.A. 0.7 objective.

RNA extraction and reverse transcription

Total RNA was extracted from cell populations collected at relevant experimental stages using the NucleospinRNA XS Kit (Macherey Nagel) according to manufacturer instructions. 1 µg of purified RNA was retro-transcribed using the iScript Advanced cDNA Synthesis Kit (Bio-Rad), which employs both oligo-dT and random primers to trigger the transcription reaction. The cDNA obtained was ready for real time-qPCR.

Real time-qPCR experiments

cDNAs retro-transcribed from hFOB RNAs were amplified performing real time-qPCR and assessed by SYBR Green fluorescence using SsoAdvanced SYBR Green Supermix (Bio-Rad Laboratories, Inc.) in a CFX Connect instrument (Bio-Rad Laboratories, Inc.). Thermal protocol and data treatment were performed as previously described (Petecchia et al. 2017). The list of genes and the sequence of forward and reverse relative primers are reported in Table 1. To obtain robust statistics, acquisitions were performed in triplicate.

Target name (function)	Primer forward	Primer reverse
Actin (housekeeping)	*CTGGAACGGTGAAGGTGACA*	*AAGGGACTTCTTGTAACAAT*
GADPH (housekeeping)	*GAAGGTGAAGGTCGGAGTC*	*GAAGATGGTGATGGGATTTC*
KDM6A (epigenetic)	*GAGGGAAGCTCTCATTGCTG*	*AGATGAGGCGGATGGTAATG*
IBSP (osteospecific)	*TCAGCCTCAGAGTCTTCATCTTC*	*GGGCAGTAGTGACTCATCCG*
BGLAP/OC (osteospecific)	*CTCACACTCCTCGCCCTATT*	*GTAGTGAAGAGACCCAGGCG*
SPP1/OP (osteospecific)	*CATCACCTGTGCCATACCAG*	*AGATGGGTCAGGGTTTAGCC*

Table 1. List of target genes used in RT-qPCR and sequence of the relative forward and reverse primers.

Quantitative phase imaging

Quantitative phase imaging (QPI) techniques were exploited to obtain quantitative reconstruction of the cell morphology and to provide high contrast images of label-free samples. In this work, two different QPI approaches were adopted: DH, which is based on interferometry, and a noncoherent method which relies on the TIE (Mir et al. 2012). DH is based on the use of a laser, a coherent source, to illuminate the sample; the phase map is recovered from the interferogram obtained by the interference of the light passing through the sample and a reference unmodified wavefront (Gabor 1948). In the present study, image acquisition has been performed through HoloMonitor M3 (Phase Holographic Imaging PHI AB, Sweden). The system is equipped with 10X magnification for phase contrast (CFI Achro, Nikon) and 20X and 40X objectives (both PlanC N, Olympus) for working with digital holography.

The method based on the TIE is non-interferometric and relays on the fact that amplitude and phase distributions are mathematically coupled in defocused images. By measuring several intensity images near the focal plane (recording a stack of defocused intensity images) it is possible to invert the equation and calculate the phase (Teague 1983). This technique benefits from operating with a standard bright-field microscope, as long as it can move along the Z axis either the sample or the objective, thus drastically reducing the cost of the optical setup. For this work, TIE resolution method has been enabled on a home-made acquisition system that integrates standard modular components (Optem FUSION, Qioptiq Photonics GmbH & Co KG), and is equipped with an Optem 10x high-resolution, long working distance (NA 0.45; WD 19 mm), infinity-corrected objective, mounted on a motorized Z-axis with a 0.01 μm resolution step. The sample is scanned through a motorized X-Y stage with a 0.5 μm resolution step. A modular, compact and freely programmable stepper motor controller (phyMOTION™, Phytron, Gröbenzell, Germany) drives three motorized axes. A LED lamp is integrated for the illumination and a Gig-E DMK 23G274 camera (The Imaging Source, Bremen, Germany) equipped with a CCD (b/w, 1600 x 1200 pixel) is used. The control software was developed in LabVIEW (National Instruments, Austin, Texas) and it automates all microscope functions such as movement of the three axes, acquisition of the 2D bright-field image and acquisition of a Z-stack of images. The number of images acquired in the Z-stack and the Z-step size can be both defined by the user. A LabVIEW module was developed for executing the algorithm producing the resulting quantitative phase images.

Image analysis

DH images were processed in order to extract shape features enabling the definition of cell populations morphological aspects. Acquired images were analysed by means of functionalities made available in M3 HStudio software (Phase Holographic Imaging PHI AB Sweden). For each image, single cells were isolated: Minimum Error Method algorithm (Kittler and Illingworth 1986),

where appropriate thresholds are selected by a minimum error criterion, demonstrated to be the most effective for segmentation, coupled to a post-processing manual error fixing. For each segmented cell the software calculates 37 different morphological parameters, including 2D morphometric indicators (such as area, perimeter, eccentricity, etc.) and parameters associated to the third dimension (such as volume, thickness, roughness, etc.). The full list of parameters extracted from cells images by HStudio software is reported in the Supplementary Materials section. In particular, according to HoloMonitor M3 image analysis software, roughness is defined as cell height irregularity and it is computed as $\acute{R} = \frac{1}{n} \cdot \sum_{i=1}^{n} |w_i - \varphi_i|$, where w is the waviness image, i.e. the smoothed version of the image, φ is the original image, all averaged over n pixels. Eccentricity measures cell elongation and it is defined as $E = \sqrt{1 - \frac{b_b^2}{a_b^2}}$, where a_b and b_b are cell diameters, respectively along major and minor axis. Irregularity measures how much cell shape deviates from a circle and it is computed as $I = 1 - \frac{4 \cdot \pi \cdot A}{p^2}$, where A is cell area and p cell perimeter. Raw data were exported, and analysed using custom Python software.

TIE images in phase-reconstructed formats were processed through a digital image correlation (DIC-like) approach in Gwyddion open-source software (Nečas et al. 2012) in order to obtain easily interpretable 3D-like images.

Elastic modulus assessment

Mechanical properties indicate how a material responds to mechanical stimuli, in particular describing how it deforms in response to an applied stress, and how this deformation evolves over time. The scaling between stress and strain of a solid material can be expressed in terms of the so-called Young's modulus (E), which indicates the ability of a material to sustain its shape under mechanical stress. A single-cell nanoindentation experiment aims at obtaining information on single cell elasticity, and is typically enabled by a calibrated force-sensing probe (commonly a µm-sized sphere) which is gently brought in contact with the cell at a constant speed. The resulting interaction force is measured as a function of the deformation of the cell, since the probe is glued to an elastic cantilever which bends proportionally to the force needed to deform the cell. Single cell elasticity value was obtained by using Piuma Chiaro (Optics11, NL), a commercial interferometric nanoindenter based on ferrule top technology (Chavan et al. 2012), adaptable to be anchored to various inverted microscopes in order to focus the cell, for this purpose attached to an Olympus IX71 inverted microscope. To measure the deflection, the Chiaro device integrates a laser interferometer, coupled to the instrument through an optical fiber. The tool can be programmed to automatically perform a grid of measurements over the cell. The probe used in this work was a glass sphere with a radius of 10.5 µm and a stiffness of 0.116 N/m, suitable for measuring objects in the range of 0.1-

100 kPa. The same probe was exploited for all tested cells, in order to allow curves comparison at different time points and experimental conditions. Cells were measured in standard Petri dishes immersed in the growing medium suitable for hFOB (described in 'Materials and methods' section), and the exploited protocol foresees to enter in contact with cells in their center, which commonly is the wider and thicker area of the cell and allows a deeper indentation. Before starting each experiment session, the optical sensitivity and the geometrical factor were calibrated using the software provided with the instrument. After each experiment the probe was washed in 70% ethanol for approximatively 10 minutes to remove eventually attached debris. Indentation curves were acquired at a speed of 2 µm/s. Curves processing, aimed at extracting a parameter related to samples mechanical properties, required the adoption of a model describing the response of the cell to the compression of the indenter. In order to obtain a robust relative evaluation of cells elasticity, the direct fit method, DFIT (Vinckier and Semenza 1998) was applied, which considers the experienced force F obtained through a perfectly rigid and spherical indenter of radius R, modeled as $F = \frac{4\sqrt{R}}{3}\frac{E}{1-\nu}\delta^{\frac{3}{2}}$ (Johnson et al., 1971) where ν is the Poisson ratio of the sample, set to 0.5 as considered suitable for cells, which are approximated to incompressible material, E its Young's modulus, and δ the indentation depth, and fits it to the collected force-versus-indentation depth curves in order to get an estimate of the Young's modulus for each cell. For excluding contribution of cell adhesion, the analysis was performed only on approach curves. All collected curves were analysed through Python custom scripts, relying on Numpy/Scipy Scientific Computing Stack (Millman and Aivazis 2011). Each dataset of curves acquired for the same experimental condition was pre-filtered to eliminate irrelevant curves (i.e. glass substrate or no substrate found) using a semi-automatic procedure. In the aim of removing the high-frequency noise and enable the determination of the tip-cell contact point, each force-indentation depth curve is filtered using Savitzky-Golay filter, and its derivative is computed. Since the tip-sample contact point is determined, the force indentation curve can be derived from the force curve. Then, force-indentation curves are fitted with DFIT on Hertz model, up to a threshold selected to match the suggested limit of the 10% of the cell thickness, and the Young's modulus can be therefore calculated.

Results

hFOB cells were induced to differentiate following the proposed protocol (see Materials and methods section) and the maturation stage towards osteoblasts was deeply characterized with reference biochemical approaches. Alizarin Red S staining was performed to visualize the amount of free calcium produced along the osteoblast mineralization process. hFOB cells in proliferation at 33.5°C were negative to the staining (Fig.1, A/AL), while a progressive increase of calcium-based

extracellular matrix was detected as sparse red spots after a few days of cell culturing at 39.5°C (Fig.1, B/AL) becoming even more evident in the following period (Fig.1, C/AL and D/AL), thus confirming the occurrence of cell maturation.

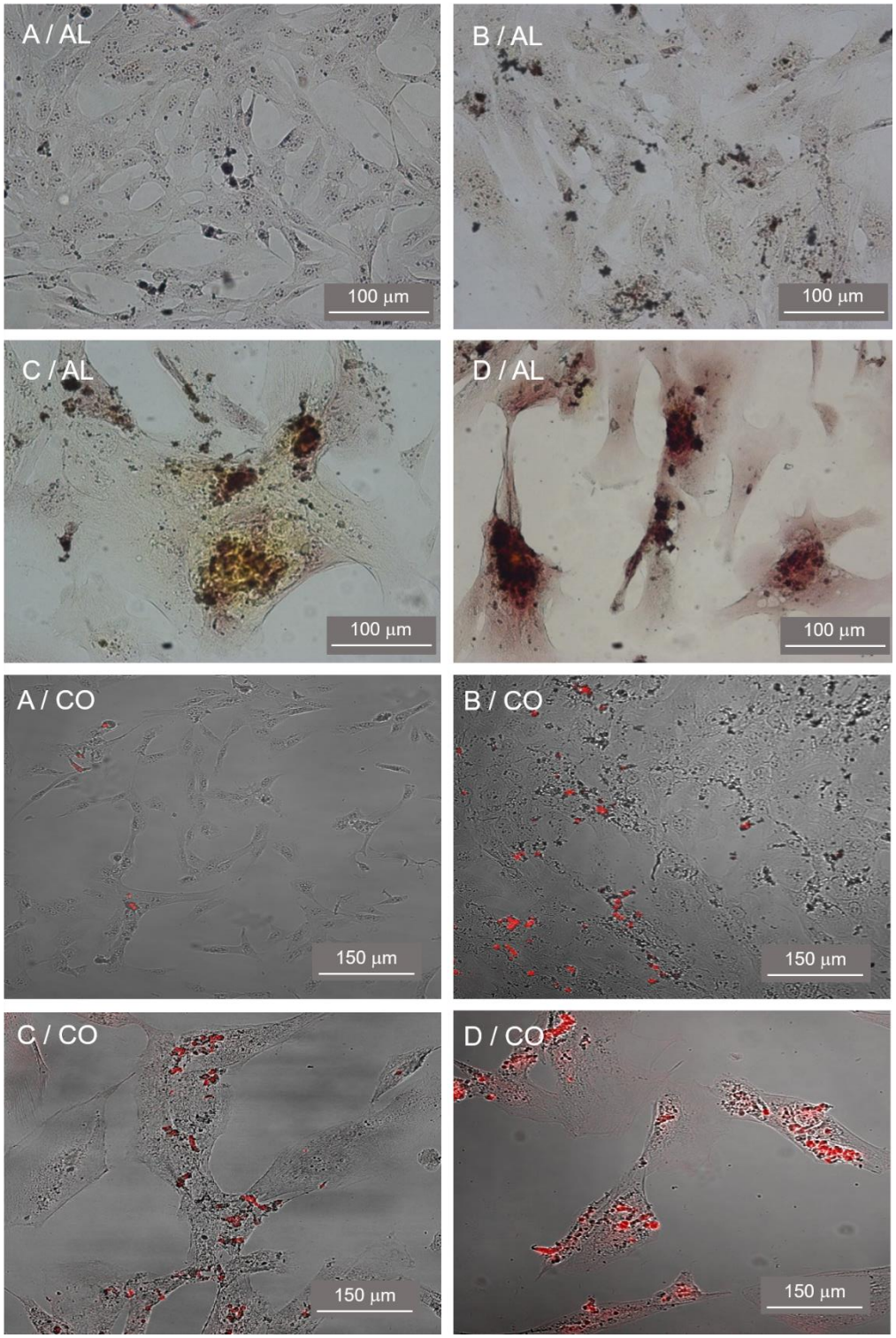

Fig.1: Summary panel reporting imaging tests on hFOB 1.19 maturation. A to D: time steps for acquisition. AL: alizarin red staining; CO: confocal microscopy acquisition of osteocalcin fluorescent staining merged with absorbance images.

The progression of osteoblast maturation is usually accompanied by changes in osteocalcin production, therefore hFOB cells were labelled with antibodies against this protein. While osteocalcin staining is barely perceptible when cells actively proliferate at 33.5°C (Fig.1, A/CO), a red fluorescence starts to be detectable after 5 days at 39.5°C (Fig.1, B/CO) and has further increment after 11 and 15 days (Fig.1, C/CO and D/CO). The visual inspection of merged fluorescence and absorbance micrograph suggests that osteocalcin is mainly localized in the perinuclear region after 5 and 11 days, while has a wider cytoplasmic distribution after 15 days.

As further confirmation of the ongoing maturation process, the expression of several bone-related genes was assessed by real time qPCR experiments. Results are summarised in in Fig.2, where target expression levels, normalized both to the housekeeping genes and to the corresponding value in proliferating cells, are indicated on the histogram bars. Tested markers included Osteocalcin (BGLAP/OC), Osteopontin (SSP1/OP), integrin binding sialoprotein (IBSP) and the histone lysine demethylase 6A (KDM6A), a chromatin epigenetic regulator. According to the generally accepted model, the first three markers are up-regulated in the second stage of osteoblast maturation, when genes connected to proliferation are down-regulated and those correlated with extra-cellular matrix (ECM) maturation are activated (Stein et al. 2004). Indeed, independent of the considered time point, all cells grown at 39.5°C show a higher expression of these markers than cells grown at 33.5°C, confirming that a maturation process is occurring. The up-regulation of KDM6A, a gene connected with stromal MSCs osteogenesis (Hemmings et al. 2014), indicates an involvement of this protein also in hFOB maturation.

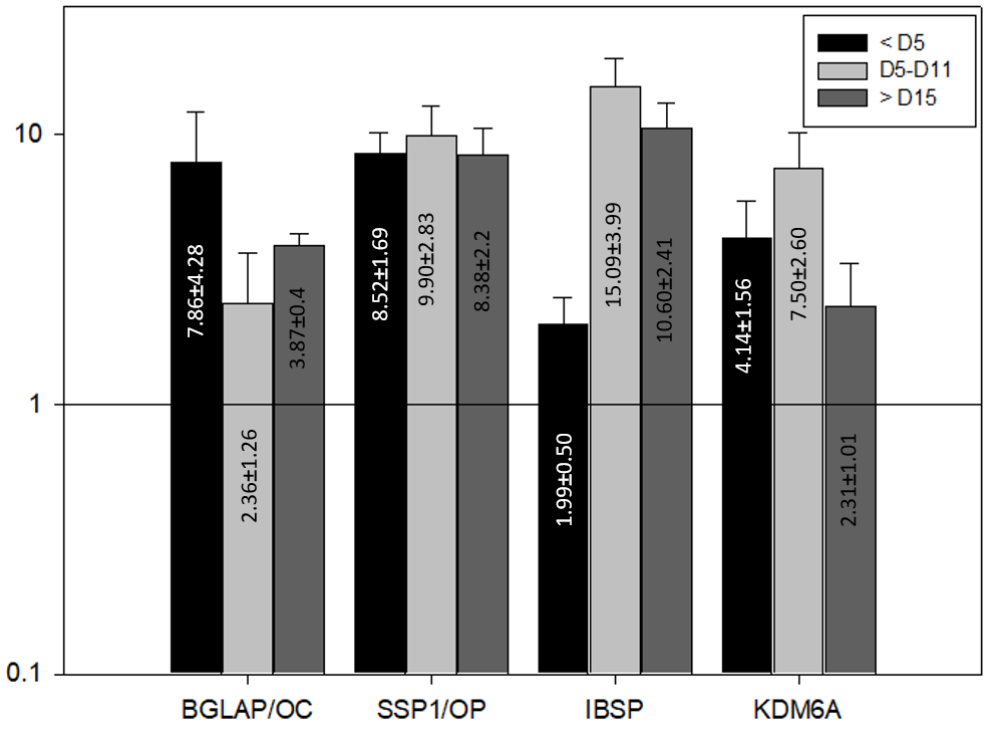

Fig.2: Histogram reporting hFOB maturation through expression of main bone-related genes assessed by qPCR. Evaluation times: less than 5 days of growth at 39.5 °C (<D5), between 5 and 11 days of growth at 39.5 °C (D5-D11), more than 15 days of growth at 39.5 °C (>D15). Expression values of target genes are shown in histogram bars.

For each growth condition, morphological and mechanical features were evaluated. These include qualitative shape knowledge from a Transport of Intensity Equation based approach (Fig.3), morphological quantitative data obtained by DH (Fig.4) and mechanical features from nanoindentation (Fig.5). Cell shape changes induced by maturation were qualitatively monitored using the 3D-like reconstruction based on QPI. This approach does not require any specialized cell treatment (no staining nor fixation) to obtain the 3D image of the cells, allowing characterization of the sample along time. Based on the acquired stack of images, a digital phase map is calculated and rendered in Fig.3 using a differential (DIC-like) filter which enhances finer details of cell morphology (McMahon et al 2002). Images reconstructed at different time steps show substantially different morphology of the cell body and appearance of the extra-cellular environment. hFOb grown at 33.5°C are smaller and narrower than mature osteoblasts grown at 39.5°C, which are wider, polygonal-shaped and whose environment shows the presence of grains in the ECM, putatively related to calcium-based release by cells.

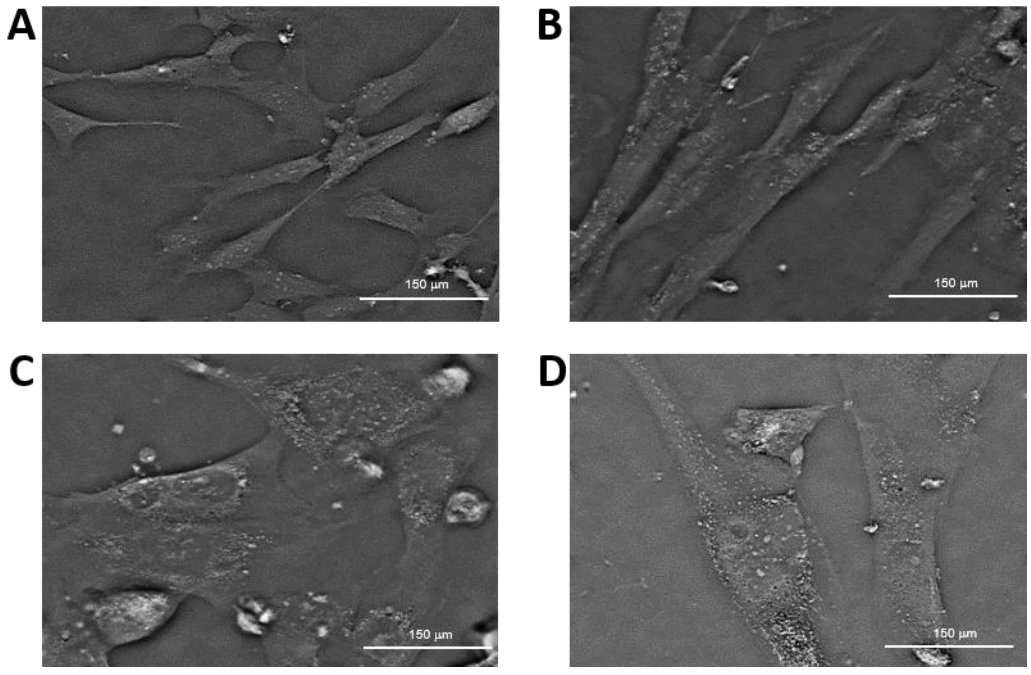

Fig.3: Images of cells morphology reconstructed using the Transport of Intensity equation during hFOB maturation (A=33,5°C, B=39,5°C for 5 days, C=39,5°C for 11 days, D=39,5°C for 15 days).

The TIE-based imaging demonstrated to be effective for qualitative characterization of cellular samples, but DH is outperforming while addressing quantitative evaluation of the different cellular features. DH was deployed to image cells at different time points along maturation, and a further

step of image processing allowed to segment and measure single cells. A typical holographic cell image obtained from this kind of experiment is reported in Fig.4A, together with a schematization of checked morphological parameters detailed in the Materials and methods section (Fig.4B).

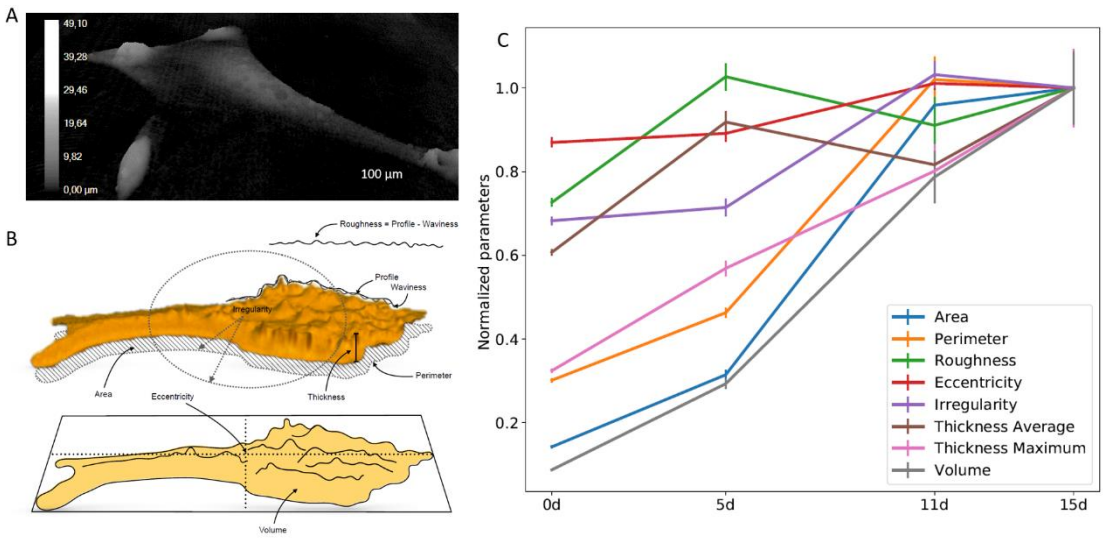

Fig.4: Digital holography. A) Example of a holographic hFOB image obtained from DH through a 20X magnification objective. B) Schematization of checked morphological parameters available through DH. C) Trends of morphological parameters changes in considered time steps (0d: proliferation condition, A; 5d: 39.5°C for 5 days, B; 11d: 39.5°C for 11 days, C; 15d: 39.5°C for 15 days, D).

Cells images were acquired in different conditions, and segmented to extract shapes' values for each cell. 296 cells from 14 images were processed for condition A; 122 cells from 21 images were processed for condition B; 20 cells from 10 images were processed for condition C; 27 cells from 14 images were processed for condition D. Average parameters, together with their standard deviation, were calculated for each condition and plotted in Fig.4C.

Consistently with knowledge from TIE, osteoblasts size increases with maturation; in each image only few, large mature cells were present when acquisition was done on samples grown for more days at 39.5°C, while a higher number of small cells was detected in each image acquired from proliferating cells.

Parameter	**Conditions**			
	A (33.5°C)	**B (39.5°C/5days)**	**C (39.5°C/11days)**	**D (39.5°C/15days)**
Area (µm²)	1365.60 ± 37.61	3039.30 ± 139.97	9038.27 ± 562.48	9702.94 ± 877.62
Eccentricity	0.80 ± 0.01	0.80 ± 0.18	0.90 ± 0.01	0.90 ± 0.01
Irregularity	0.40 ± 0.01	0.40 ± 0.01	0.65 ± 0.20	0.62 ± 0.02
ThicknessMax (µm)	3.77 ± 0.08	6.64 ± 0.28	9.53 ± 1.02	12.03 ± 1.38
ThicknessAvg (µm²)	1.21 ± 0.02	1.89 ± 0.07	1.62 ± 0.08	2.07 ± 0.19
Perimeter (µm)	174.55 ± 3.37	266.97 ± 8.78	591.77 ± 35.2	578.25 ± 34.01
RoughnessAvg (µm)	4.17 ± 0.08	5.98 ± 0.25	5.12 ± 0.41	5.71 ± 0.49
Volume (µm3)	1671.60 ± 56.89	5510.84 ± 273.50	14716.45 ± 1293.01	19351.20 ± 2149.43

Table 2: Average values of morphological parameters exploited in the analysis, and related SEM.

Cell elastic modulus was measured for each time point following the procedure previously described. For each experimental condition, around 150 indentation curves were acquired, repeating acquisitions at least 3 times for each cultured condition. Measurements were performed at room temperature and the indentations were collected for less than 1 hour for each cell plate, in order to preserve the stability of the sample. A typical force-displacement curve obtained from this experiment is reported in Fig.5A.

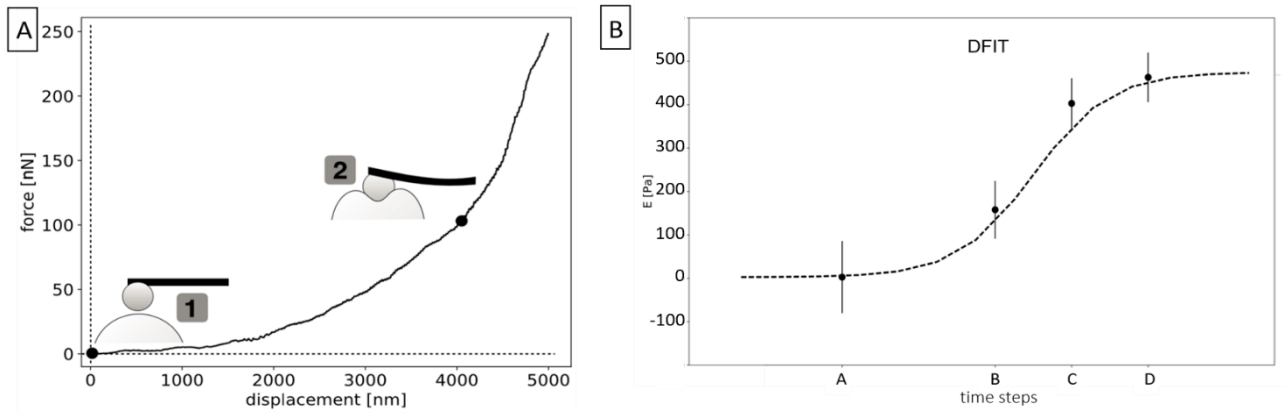

Fig.5: Nanoindentation. A) Force-displacement curve of the indentation phase. In step '1' Chiaro probe is approaching the cell; step '2' represents cell indentation and associated cantilever bending. B) Average elastic modulus measured during hFOB maturation. Results are obtained from DFIT approach applied to nanoindentation curves; the dashed curve represents a best fit with a sigmoidal trend and it is included as a guide to the eyes.

Fig.5B shows the average elastic modulus (E) measured during hFOB maturation and calculated using the DFIT approach. Relative values are shown, considering as reference value obtained for condition A (E=2400Pa). The obtained results clearly show a tendency of cells to get more rigid with maturation, with a marked increase during the initial steps (points A, B, C), followed by a saturation phase (point D), where values are quite constant.

Trends of morphometric and elastic features during time steps have been correlated pairwise, using Pearson correlation index calculated using Python Pandas library (https://pandas.pydata.org): results are shown in a correlation matrix reported in Fig.6.

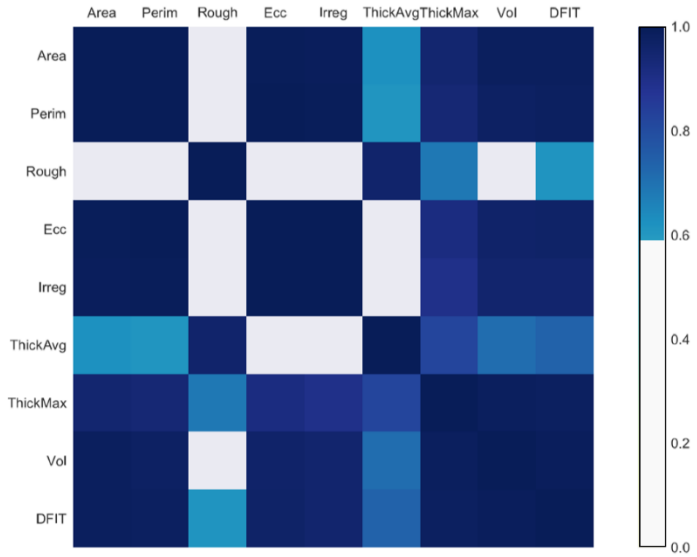

Fig.6: Correlation matrix of considered parameters over time: it measures the correlation of elasticity trend during hFOB maturation with trends of the analysed morphometric features. Only values showing r>0.6 are shown.

Discussion and conclusion

Bone is a dynamic tissue, constantly being reshaped. Osteoblasts, which are the major cellular component of this tissue, are responsible for producing and secreting matrix proteins and transporting mineral into the matrix, which will be broken down by osteoclasts in the tissue remodelling process. Osteoblasts derive from mesenchymal stem cells (MSCs), which are also able to give rise to adipose or cartilage cells. When osteoblasts are buried and immobilized into extracellular matrix they become osteocytes. During their journey from MSCs to osteocytes, osteoblasts undertake diverse functional conditions, and monitoring their maturation is crucial for assessing bone tissue formation, which represent the basis for bone-related diseases studies and bone tissue regeneration approaches. A number of techniques are commonly exploited in order to evaluate osteoblasts stage of maturation. Most of them make use of chemical or biochemical labels, such as alizarin red for detecting Ca^{2+} production (Putchler et al. 1969) or fluorescent dyes for revealing osteocalcin (BGLAP) presence (Tsao et al. 2017), to detect the presence of specific molecules in the extracellular matrix (ECM) surrounding osteoblasts. Other approaches involve the use of qPCR to evaluate transcription levels of targets known to be differently expressed in diverse stages of osteoblast maturation, such as IBSP, OP and OC (Setzer et al. 2009). However, label-free techniques, which could represent faster and user-friendly approaches, did not enter yet the common lab practices.

In this paper a label-free morpho-mechanics approach for assessing osteoblasts maturation relying on morphological and mechanical modifications is presented. It is recognized that both morphological and mechanical properties of living cells are associated with their structural

characteristics (Yang et al. 2016; Atilgan et al. 2005) and their functional state, and their study contributes to understand and evaluate, among the others, drug treatment effects (Pasqualato et al. 2012), immune cell activation (Lin et al. 2015), cell differentiation (Petecchia et al. 2017) and cancer prognosis (Efremov et al. 2014). For example, alterations in cell cytoskeletal architecture have direct effects not only on cell morphology (Fletcher et al 2010) but even on organelles organization (Bershadsky and Vasiliev 1988), cytoplasmic trafficking (Willmann and Dringen 2018), cell adhesion (Parsons et al. 2010), migration (Tang and Gerlach 2017), polarization (Raman et al. 2018), and differentiation (Müller et al. 2013), thus modulating status and health. In this context, cell shape phenotype and mechanotype are emerging as valuable label-free biomarkers. In this work mechanical properties were assessed through single-cell nanoindentation, while morphological parameters were acquired and estimated through digital holography, an interferometric approach able to provide label-free 2D and 3D single-cell shape features. hFOB 1.19 cell line was chosen as model for bone cells, not only because it is a well characterized cell line (Harris et al. 1995, Setzer et al. 2009), but also for its unique and intrinsic feature of evolving from pre-osteoblasts to pre-osteocytes depending on temperature and time of culture. Its maturation state was assessed by traditional qualitative staining (Alizarin Red staining and osteocalcin fluorescent labelling) and quantitative gene expression (qPCR) systems. Using innovative technologies (DH, TIE, single cell nanoindentation), hFOB morpho-mechanical phenotypes were analysed at different time points of maturation, thus concurrently assessing their cellular functionality and morpho-mechanical characteristics.

Results show that hFOB morpho-mechanical features are highly correlated to their physiological stage (Fig.6), thus representing promising label-free tools able to check osteoblast maturation. It was expected that mechanical properties could play a relevant role in cell life and function: actually, basic processes such as cell growth, proliferation, migration, adhesion, and differentiation, all depend on and are regulated by mechanical properties (Titushkin et al. 2007). In recent studies the definition of living cell stiffness proved to be a biophysical fingerprint able to discern between cell phenotypes, to unravel processes in aging or diseases, to detect and diagnose pathological status of cell (Lim et al. 2011, Mescola et al. 2012, Lee et al. 2016, Northcott et al. 2018, Scholz et al. 2018, Harris et al. 2018, Zemła et al. 2018). Since elastic modulus enormously depends on exploited technology and chosen probe (Wu et al. 2018) and absolute data between different experiments are often highly incomparable between different experiments, the most appropriate way to show evolution of this parameter during hFOB maturation appeared to be the increment with respect to the initial condition value. hFOB stiffness, which appeared in line with literature findings (Docheva et al. 2008, Kelly et al. 2011), increases of about 450 Pa during cells maturation process, following a trend that can be fitted on a sigmoidal curve (Fig.5B).

For what concerns morphology features, scientific literature even shows that cell shape can be associated to functional and health status (Baba et al. 2007, Petecchia et al. 2017). Testing hFOB, both qualitative TIE and quantitative holographic images highlight important changes in cells morphology (Fig.3 and Table 2). Morphology changes can be associated to differentiation toward mature osteoblasts, thus expressing the normal osteoblast phenotype, characterized by large, flat and polygonally- shaped cells surrounded from calcium-based grains. It is worth noticing that some shape characteristics of hFOB evolve in temperature and time with trends analogous to the elastic behaviour, leading to hypothesize that consistent cytoskeletal and internal organelles remodelling impact not only on cell morphology and behaviour, but also on mechanical properties. In particular, the evolution of osteoblasts stiffness, acquired over time in proliferation and maturation modes, results to be highly correlated ($r>0.9$) with modification in osteoblasts occupancy area, perimeter, eccentricity factor, surface irregularity, maximum thickness and volume (Fig.6).

In conclusion, the present work provides a detailed study of the changes of the morpho-mechanical phenotype of hFOB cells along their maturation from pre-osteoblasts to mature osteoblasts. Although the chosen cellular system is a genetically designed model, only partially recapitulating the complexity of the original bone tissue (Rutkovskiy et al. 2016), this work suggests that morphological and elastic properties can represent a relevant marker to follow osteoblasts during their maturation process. The presented study provides an indication of a connection between the physical properties of the cell and the ability to develop towards a mature bone tissue. Although the proposed measurements intend to highlight a statistical link between cell morpho-mechanics and its maturation stage, a biomolecular interpretation of findings can be hypothesised. In particular, recent results by Li et al. (2019) and Sun et al. (2019) shed additional light on the mechano-transduction processes activated in the bone (Shuaib et al. 2019, Alfieri et al. 2019), clearly demonstrating a central role of the mechanosensitive ion channel Piezo1 in bone formation and anabolism in animal systems. The knockout of Piezo1, a very peculiar molecule capable of directly sensing and transducing mechanical stimuli, thus determining the fate of differentiating mesenchymal stem cells (Sugimoto et al. 2017), severely impairs bone structure and strength. This mechano-transduction process influences and is potently influenced by the organization of the cytoskeleton (Cox et al. 2016) and the biomechanics of the cell and of the underlying environment (Bavi et al. 2019). The findings of the present paper can be interpreted in this scenario, directly connecting the cell mechano-type and its biological fate: the possibility to characterize morpho-mechanical aspects using advanced biophysical tools opens the way for a fine measurement of the maturation of osteoblasts in patho-physiologically relevant contexts.

Acknowledgements
This work was supported by the Ministry of Education, Universities and Research of Italy, in the context of the FIRB 'Futuro in Ricerca 2013' project [grant number RBFR13V4M2]. Thanks to Francesca Quartino for technical support.

Reference

1. Alfieri R, Vassalli M, Viti F. Flow-induced mechanotransduction in skeletal cells. Biophys Rev. 2019, 11(5):729-743.
2. Ambühl ME, Brepsant C, Meister JJ, Verkhovsky AB, Sbalzarini IF. High-resolution cell outline segmentation and tracking from phase-contrast microscopy images. J Microsc. 2012, 245(2):161-70. doi: 10.1111/j.1365-2818.2011.03558.x.
3. Atilgan E, Wirtz D, Sun SX. Morphology of the lamellipodium and organization of actin filaments at the leading edge of crawling cells. Biophys J. 2005 Nov;89(5):3589-602.
4. Baba AI, Câtoi C. Comparative Oncology. Bucharest: The Publishing House of the Romanian Academy. 2007. Chapter 3, Tumor Cell Morphology.
5. Bavi N, Richardson J, Heu C, Martinac B, Poole K. PIEZO1-Mediated Currents Are Modulated by Substrate Mechanics. ACS Nano. 2019, 13(11):13545-13559.
6. Bershadsky A.D., Vasiliev J.M. (1988) Cytoskeleton and Internal Organization of the Cell. In: Cytoskeleton. Cellular Organelles. Springer, Boston, MA
7. Binnig G, Quate CF and Gerbe Ch. Atomic Force Microscope. Physical Review Letters. 1986, 56(9):930-934.
8. Brodland GW and Veldhuis JH. The Mechanics of Metastasis: Insights from a Computational Model. PLoS One. 2012, 7(9):e44281.
9. Chang L, Ni J, Beretov J, Wasinger VC, Hao J, Bucci J, Malouf D, Gillatt D, Graham PH, Li Y. Identification of protein biomarkers and signaling pathways associated with prostate cancer radioresistance using label-free LC-MS/MS proteomic approach. Scientific Reports. 2017, 7:41834.
10. Chavan D, van de Watering TC, Gruca G, Rector JH, Heeck K, Slaman M, Iannuzzi D. Ferrule-top nanoindenter: an optomechanical fiber sensor for nanoindentation. Rev Sci Instrum. 2012, 83(11):115110.
11. Chen J, Huang SB, Xue C, Fan B, Chen D, Wang J, Wu MH. Single-Cell Mechanical Properties: Label-Free Biomarkers for Cell Status Evaluation. In: Tseng FG., Santra T. (eds) Essentials of Single-Cell Analysis. Series in BioEngineering. Springer, Berlin, Heidelberg. 2016, 213-234.
12. Cox C, Bae C, Ziegler L, Hartley S, Nikolova-Krstevski V, Rohde PR, Ng CA, Sachs F, Gottlieb PA, Martinac B. Removal of the mechanoprotective influence of the cytoskeleton reveals PIEZO1 is gated by bilayer tension. Nat Commun. 2016, 7:10366.
13. Darling EM and Di Carlo D. High-Throughput Assessment of Cellular Mechanical Properties. Annu Rev Biomed Eng. 2015, 17:35-62.
14. Docheva D, Padula D, Popov C, Mutschler W, Clausen-Schaumann H, Schieker M. Researching into the cellular shape, volume and elasticity of mesenchymal stem cells, osteoblasts and osteosarcoma cells by atomic force microscopy. J Cell Mol Med. 2008, 12(2):537–552.
15. Efremov YM, Lomakina ME, Bagrov DV, Makhnovskiy PI, Alexandrova AY, Kirpichnikov MP, Shaitan KV. Mechanical properties of fibroblasts depend on level of cancer transformation. Biochim Biophys Acta. 2014 May;1843(5):1013-9. doi: 10.1016/j.bbamcr.2014.01.032.
16. Engler AJ1, Sen S, Sweeney HL, Discher DE. Matrix elasticity directs stem cell lineage specification. Cell. 2006, 126(4):677-89.
17. Fletcher DA, Mullins RD. Cell mechanics and the cytoskeleton. Nature. 2010, 463(7280):485-92.
18. Ford J. Red blood cell morphology. Int J Lab Hematol. 2013 Jun;35(3):351-7.
19. Fortier H, Variola F, Wang C and Zou S. AFM force indentation analysis on leukemia cells. Anal. Methods. 2016, 8:4421-4431.
20. Gabor D. A new microscopic principle. Nature. 1948, 161:777-778.
21. Golfier S, Rosendahl P, Mietke A, Herbig M, Guck J, Otto O. High-throughput cell mechanical phenotyping for label-free titration assays of cytoskeletal modifications. Cytoskeleton (Hoboken). 2017, 74(8):283-296. doi: 10.1002/cm.21369.
22. Harris MJ, Wirtz D, Wu PH. 2018. Dissecting cellular mechanics: Implications for aging, cancer, and immunity. Semin Cell Dev Biol. pii: S1084-9521(18)30143-5.

23. Harris SA, Enger RJ, Riggs BL, Spelsberg TC. Development and characterization of a conditionally immortalized human fetal osteoblastic cell line. Journal of Bone and Mineral Research. 1995, 10(2):178-186.
24. Hemming S, Cakouros D, Isenmann S, Cooper L, Menicanin D, Zannettino A, Gronthos S. EZH2 and KDM6A act as an epigenetic switch to regulate mesenchymal stem cell lineage specification. Stem Cells. 2014, 32(3):802-15. doi: 10.1002/stem.1573.
25. Johnson KL, Kendall K, Roberts AD, Tabor D. Surface energy and the contact of elastic solids. Proceedings of the Royal Society of London. A. Mathematical and Physical Sciences. 1971, 324(1558).
26. Kawano S, Kojima M, Higuchi Y et al. Assessment of elasticity of colorectal cancer tissue, clinical utility, pathological and phenotypical relevance. Cancer Sci. 2015, 106(9):1232-1239.
27. Kelly GM, Kilpatrick JI, van Es MH, Weafer PP, Prendergast PJ, Jarvis SP. Bone cell elasticity and morphology changes during the cell cycle. Journal of Biomechanics. 2011, 44(8):1484-1490.
28. Kittler J and Illingworth J. Minimum error thresholding. Pattern Recognition. 1986, 19(1):41-47.
29. Kumar S, Weaver VM. Mechanics, malignancy, and metastasis: the force journey of a tumor cell. Cancer Metastasis Rev. 2009, 28(1-2):113-127.
30. Lee CW, Jang LL, Pan HJ, Chen YR, Chen CC, Lee CH. Membrane roughness as a sensitive parameter reflecting the status of neuronal cells in response to chemical and nanoparticle treatments. Journal of Nanobiotechnology. 2016, 14:9.
31. Li X, Han L, Nookaew I, Mannen E, Silva MJ, Almeida M, Xiong J. Stimulation of Piezo1 by mechanical signals promotes bone anabolism. Elife. 2019, 8. pii: e49631.
32. Lim CT, Li A. Mechanopathology of red blood cell diseases — Why mechanics matters. Theoretical and Applied Mechanics Letters. 2011, 1(1):014000.
33. Lin W, Suo Y, Deng Y, Fan Z, Zheng Y, Wei X, Chu Y. Morphological change of CD4(+) T cell during contact with DC modulates T-cell activation by accumulation of F-actin in the immunology synapse. BMC Immunol. 2015 Aug 26;16:49. doi: 10.1186/s12865-015-0108-x.
34. Lulevich V, Zink T, Chen HY, Liu FT, Liu GY. Cell Mechanics Using Atomic Force Microscopy-Based Single-Cell Compression. Langmuir. 2006, 22(19):8151–8155.
35. McMahon PJ, Barone-Nugent ED, Allman BE, Nugent KA. Quantitative phase-amplitude microscopy II: differential interference contrast imaging for biological TEM. J Microsc. 2002, 206(Pt 3):204-8.
36. Mescola A, Vella S, Scotto M, Gavazzo P, Canale C, Diaspro A, Pagano A, Vassalli M. Probing cytoskeleton organisation of neuroblastoma cells with single-cell force spectroscopy. J Mol Recognit. 2012, 25(5):270-7.
37. Millman KJ and Aivazis M. Python for Scientists and Engineers. Computing in Science & Engineering. 2011, 13(2):9-12.
38. Mir M, Bhaduri B, Wang R, Zhu R, Popescu G. Quantitative Phase Imaging. Prog Opt. 2012, 57:133-217.
39. Monteiro JM, Fernandes PB, Vaz F, Pereira AR, Tavares AC, Ferreira MT, Pereira PM, Veiga H, Kuru E, VanNieuwenhze MS, Brun YV, Filipe SR & Pinho MG. Cell shape dynamics during the staphylococcal cell cycle. Nature Communications. 2015, 6:8055.
40. Müller P, Langenbach A, Kaminski A, Rychly J. Modulating the actin cytoskeleton affects mechanically induced signal transduction and differentiation in mesenchymal stem cells. PLoS One. 2013 Jul 29;8(7):e71283. doi: 10.1371/journal.pone.0071283.
41. Muthukumaran P, Lim CT, Lee T. Estradiol influences the mechanical properties of human fetal osteoblasts through cytoskeletal changes. Biochem Biophys Res Commun. 2012; 423(3):503-8. doi: 10.1016/j.bbrc.2012.05.149.
42. Nečas D, Klapetek P. Gwyddion: an open-source software for SPM data analysis. Cent Eur J Phys. 2012, 10: 181-188.
43. Northcott JM, Dean IS, Mouw JK, Weaver VM. Feeling Stress: The Mechanics of Cancer Progression and Aggression. Front Cell Dev Biol. 2018, 6:17.
44. Parsons JT, Horwitz AR, Schwartz MA. Cell adhesion: integrating cytoskeletal dynamics and cellular tension. Nat Rev Mol Cell Biol. 2010 Sep;11(9):633-43. doi: 10.1038/nrm2957.
45. Pasqualato A, Palombo A, Cucina A, Mariggiò MA, Galli L, Passaro D, Dinicola S, Proietti S, D'Anselmi F, Coluccia P, Bizzarri M. Quantitative shape analysis of chemoresistant colon cancer cells: correlation between morphotype and phenotype. Exp Cell Res. 2012 Apr 15;318(7):835-46. doi: 10.1016/j.yexcr.2012.01.022.
46. Petecchia L, Sbrana F, Utzeri R, Vercellino M, Usai C, Visai L, Vassalli M, Gavazzo P. Electro-magnetic field promotes osteogenic differentiation of hMSC through a selective action on Ca2+-related

mechanisms. Sci Rep. 2015, 5:13856.
47. Petecchia L, Viti F, Sbrana F, Vassalli M, Gavazzo P. A biophysical approach to quantify skeletal stem cells trans-differentiation as a model for the study of osteoporosis. Biophys Chem. 2017, 229:84-92.
48. Putchler H, Meloan S, Terry MA. On the history and mechanism of alizarin and alizarin red S stains for calcium. J. Histochem. Cytochem. 1969, 17:110-124.
49. Raman R, Pinto CS, Sonawane M. Polarized Organization of the Cytoskeleton: Regulation by Cell Polarity Proteins. J Mol Biol. 2018 Sep 28;430(19):3565-3584. doi: 10.1016/j.jmb.2018.06.028.
50. Ray P and Steckl AJ. Label-Free Optical Detection of Multiple Biomarkers in Sweat, Plasma, Urine, and Saliva. ACS Sens. 2019. doi: 10.1021/acssensors.9b00301.
51. Rutkovskiy A, Stensløkken KO, Vaage IJ. Osteoblast Differentiation at a Glance. Med Sci Monit Basic Res. 2016, 22:95-106.
52. Scholz N. Cancer Cell Mechanics: Adhesion G Protein-coupled Receptors in Action? Front Oncol. 2018, 8: 59.
53. Setzer B, Bachle M, Metzger MC, Kohal RJ. The gene-expression and phenotypic response of hFOB 1.19 osteoblasts to surface-modified titanium and zirconia. Biomaterials. 2009, 30:979–990.
54. Shuaib A, Motan D, Bhattacharya P, McNabb A, Skerry TM, Lacroix D. Heterogeneity in The Mechanical Properties of Integrins Determines Mechanotransduction Dynamics in Bone Osteoblasts. Sci Rep. 2019, 9:13113.
55. Stein GS, Lian JB, van Wijnen AJ, Stein JL, Montecino M, Javed A, Zaidi SK, Young DW, Choi JY, Pockwinse SM. Runx2 control of organization, assembly and activity of the regulatory machinery for skeletal gene expression. Oncogene. 2004, 23(24):4315-29.
56. Stern E, Vacic A, Rajan NK, Criscione JM, Park J, Ilic BR, Mooney DJ, Reed MA, Fahmy TM. Label-free biomarker detection from whole blood. Nature nanotechnology. 2009, 5(2), 138–142. doi:10.1038/nnano.2009.353
57. Sugimoto A, Miyazaki A, Kawarabayashi K, Shono M, Akazawa Y, Hasegawa T, Ueda-Yamaguchi K, Kitamura T, Yoshizaki K, Fukumoto S, Iwamoto T. Piezo type mechanosensitive ion channel component 1 functions as a regulator of the cell fate determination of mesenchymal stem cells. Sci Rep. 2017, 7:17696.
58. Sun W, Chi S, Li Y, Ling S, Tan Y, Xu Y, Jiang F, Li J, Liu C, Zhong G, Cao D, Jin X, Zhao D, Gao X, Liu Z, Xiao B, Li Y. The mechanosensitive Piezo1 channel is required for bone formation. Elife. 2019 Jul 10;8. pii: e47454.
59. Tang DD, Gerlach BD. The roles and regulation of the actin cytoskeleton, intermediate filaments and microtubules in smooth muscle cell migration. Respir Res. 2017 Apr 8;18(1):54. doi: 10.1186/s12931-017-0544-7.
60. Teague MR . Deterministic phase retrieval: a Green's function solution. J Opt Soc Am. 1983, 73:1434-1441.
61. Thompson WR, Rubin CT, Rubin J. Mechanical regulation of signaling pathways in bone. Gene. 2012, 503:179–193.
62. Titushkin I and Cho M. Distinct Membrane Mechanical Properties of Human Mesenchymal Stem Cells Determined Using Laser Optical Tweezers. Biophys J. 2006, 90(7):2582–2591.
63. Titushkin I and Cho M. Modulation of Cellular Mechanics during Osteogenic Differentiation of Human Mesenchymal Stem Cells. Biophysical Journal. 2007, 93(10):3693-3702.
64. Tsao YT, Huang YJ, Wu HH, Liu YA, Liu YS, Lee OK. Osteocalcin Mediates Biomineralization during Osteogenic Maturation in Human Mesenchymal Stromal Cells. Int J Mol Sci. 2017, 18(1):159.
65. Vinckier A and Semenza G. Measuring elasticity of biological materials by atomic force microscopy. FEBS Lett. 1998, 430(1-2):12-6.
66. Willmann W, Dringen R. Monitoring of the Cytoskeleton-Dependent Intracellular Trafficking of Fluorescent Iron Oxide Nanoparticles by Nanoparticle Pulse-Chase Experiments in C6 Glioma Cells. Neurochem Res. 2018 Nov;43(11):2055-2071. doi: 10.1007/s11064-018-2627-3.
67. Wu PH, Phillip JM, Khatau SB, Chen WC, Stirman J, Rosseel S, Tschudi K, Van Patten J, Wong M, Gupta S, Baras AS, Leek JT, Maitra A, Wirtz D. Evolution of cellular morpho-phenotypes in cancer metastasis. Scientific Reports 2015, 5:18437.
68. Wu PH, Aroush DRB, Asnacios A, Chen WC, Dokukin ME, Doss BL, Durand-Smet P, Ekpenyong A, Guck J, Guz NV, Janmey PA, Lee JSH, Moore NM, Ott A, Poh YC, Ros R, Sander M, Sokolov I, Staunton JR, Wang N, Whyte G, Wirtz D. A comparison of methods to assess cell mechanical properties. Nature Methods. 2018, 15:491–498.
69. Yang DC, Blair KM, Salama NR. 2016. Staying in shape: the impact of cell shape on bacterial survival

in diverse environments. Microbiol Mol Biol Rev 80:187-203. doi:10.1128/MMBR.00031-15.
70. Yen ML, Chien CC, Chiu IM, Huang HI, Chen YC, Hu HI, Yen BL. Multilineage differentiation and characterization of the human fetal osteoblastic 1.19 cell line: a possible in vitro model of human mesenchymal progenitors. Stem Cells. 2007 Jan;25(1):125-31.
71. Zemła J, Danilkiewicz J, Orzechowska B, Pabijan J, Seweryn S, Lekka M. Atomic force microscopy as a tool for assessing the cellular elasticity and adhesiveness to identify cancer cells and tissues. Semin Cell Dev Biol. 2018, 73:115-124.
72. Zhang J, Moradi E, Somekh MG & Mather ML. Label-Free, High Resolution, Multi-Modal Light Microscopy for Discrimination of Live Stem Cell Differentiation Status. Scientific Reports. 2018, 8:697.